Mechanism of directional emission from a peanut-shaped microcavity

Fang-Jie Shu, Chang-Ling Zou, Fang-Wen Sun, and Yun-Feng Xiao

Phys. Rev. A **83**, 053835 — Published 26 May 2011

DOI: 10.1103/PhysRevA.83.053835

Mechanism of directional emission from a peanut-shaped microcavity

Fang-Jie Shu[1,2*], Chang-Ling Zou[3], Fang-Wen Sun[3], and Yun-Feng Xiao[2*]

[1]*Department of Physics, Shangqiu Normal University, Shangqiu 476000, P. R. China*

[2]*State Key Lab for Mesoscopic Physics and Department of Physics, Peking University, Beijing 100871, P. R. China*

[3]*Key Laboratory of Quantum Information, University of Science and Technology of China, Hefei, Anhui 230026, P. R. China*

Abstract:

Collimated directional emission is essentially required for an asymmetric resonant cavity. In this paper, we theoretically investigate a type of peanut-shaped microcavity which can support highly directional emission with the beam divergence as small as 2.5^{o}. The mechanism of the collimated emission of this type of peanut-shaped microcavity is explained with the short-term ray trajectory. Moreover, the explanations are also confirmed by the numerical wave simulation. This extremely narrow divergence of the emission holds a great potential in highly collimated lasing from on-chip microcavities.

PACS numbers: 05.45.Mt, 42.25.-p, 42.60.Da

* Email address: shufangjie@gmail.com
* URL: www.phy.pku.edu.cn/personnel/imo/yfxiao; Email address: yfxiao@pku.edu.cn

I. Introduction

Whispering-gallery modes (WGMs) in microcavity systems with rotational symmetry are of current interest owing to their high quality factor (Q) values and small mode volumes at optical frequencies. WGMs are considered the most promising candidates for a large variety of optical applications, ranging from ultralow-threshold lasing, highly sensitive sensing, to cavity quantum electrodynamics [1]. An important drawback of WGMs is their isotropic emissions due to the inherently rotational symmetry. This causes a significant difficulty to efficiently excite the cavity modes and collect the microcavity emission for practical purposes. A natural choice is to design the geometrical shape of microcavities for producing a strongly directional output. These resonators are known as asymmetric resonant cavities (ARCs) or deformed cavities [2]. Actually, shortly after the first fabrication of microdisk it was demonstrated that deforming of boundary improves directionality of emission [3-5]. Since then, ARCs with directional emissions have been demonstrated in various systems: quadrupolar microdisks [5-7], full-chaos microstadiums [8-10], spiral-shape micropillars [11] or microdisks [12], quadrupolar liquid jet [13, 14], limaçon shaped microdisks [15, 16], and three-dimensional deformed microspheres [17, 18].

Output beam divergence is an important property for ARCs, because it determines not only a high-brightness laser spot but also a high coupling efficiency. The divergence can be estimated from the full width at half maximum (FWHM) of emission peaks in the far-field patterns (FFPs). In most ARCs [5, 7, 10-13, 15, 18], the divergence angle typically ranges from 10^o to 30^o. The divergence angle exceeds 30^o for limaçon shaped microdisks [15, 16]. Only a special microstadium in Ref. [9] reported the divergence angle with several degrees. To obtain a

minimized divergence, Shang et al. studied a peanut-shaped cavity in which the divergence of directional emission approached 2^o [19]. Therein, the authors explained experimental results with a hybrid WGM-two-bouncing orbit (a closed loop forms with a whispering gallery orbit and a two-bouncing orbit), and they credited the collimation mainly to the two-bouncing orbit. Nevertheless, this orbit cannot be considered as the only possible obit before further theoretical investigating. In this research, we aim to theoretically reveal the mechanism of collimated emission from the peanut-shaped microcavity. In Section II, a brief description of the shape setting and the Poincaré surface of section (SOS) of the peanut-shaped microcavity are provided. In Section III, we obtain the FFPs of different shapes of peanut, and then focus on ray trajectory of a typical peanut-shaped cavity. In Section IV, the wave method is employed to find the double-pentagon modes and confirm the ray result. Finally, in Section V, the refractive index of the microcavity material is discussed to optimize the emission property of the cavity.

II. Geometry of the peanut-shaped microcavity

The geometry of the peanut-shaped microcavity (two-dimensional) is shown in Fig. 1(a) (shadow part). It consists of two contacted identical microdisks $C_{1,2}$ with radius of r_1 and a central region between them. The boundary of the central region is defined by the other two identical microdisks $C_{3,4}$ with radius of r_2 which are tangential to $C_{1,2}$. The whole boundary of the cavity is continuous and smooth. It looks like a peanut, thus named as a peanut-shaped microcavity.

In this design, the angle $\beta = \arccos(r_1/(r_1+r_2))$ can describe the geometry of the

peanut-shaped microcavity. Here, as a morphological parameter β ranges from 0 to 90 degrees. When $\beta = 0^o$, the peanut-shaped cavity is reduced to double disks in contact, which is also called photonic molecule being extensively studied recently [20]. When $\beta = 90^o$, the peanut-shaped cavity becomes a microstadium. For $0^o < \beta < 90^o$, it is a general peanut shape studied in this paper. It should be noted that the present shaped microcavity is made of the same material with uniform refraction index n, which is slightly different from Ref. [19] where two silica cylinders are coated by a hybrid glass material. In Fig. 1(a), s stands for the curvilinear coordinate along the boundary, and φ denotes the far field angle measured from the main axis of the peanut.

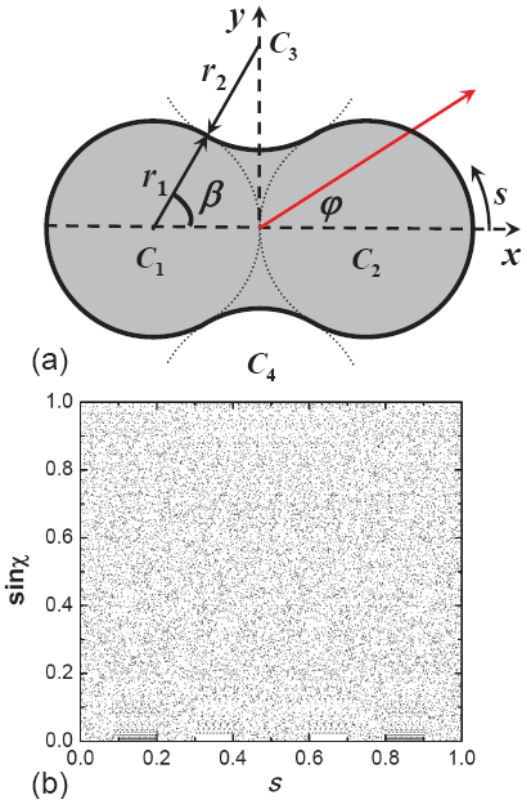

Fig. 1. (Color online) (a) Peanut-shaped microcavity (shadow). Here, s stands for the curvilinear coordinate along the boundary, β describes the shape setting angle, and φ denotes the far-field angle measured from the main axis of the peanut. (b) The SOS of the closed peanut-shaped microcavity with $\beta = 60°$.

III. Ray dynamics in the peanut-shaped microcavity

Ray dynamics provides an intuitive and efficient tool to understand the emission properties of a deformed microcavity [7]. Thus, we first calculate the SOS of the closed peanut-shaped microcavity (the billiard) with $\beta = 60^{o}$ as plotted in Fig. 1(b). To obtain the SOS, forty rays with different initial conditions successively reflect on the microcavity boundary, where the ray tracing is recorded by the coordinate of reflection point (s, $|\sin\chi|$). Here χ represents the angle of incidence. It can be found that the ray dynamics in the SOS is fully chaotic, indicating no stable trajectory for light existed in the peanut cavity.

In the ray optics model, the ray dynamics depends on the incident angle χ. When χ is larger than the critical refraction angle $\chi_c = \arcsin(1/n)$, the ray undergoes total internal reflection. Otherwise, the ray splits into a reflective and a refractive rays and the intensity of each part is decided by Fresnel's law [21]. For simplicity but without loss of the generality, we concentrate on the transverse magnetic (TM) polarized modes, whose electric field and the corresponding normal derivative are continuous crossing the boundary. Assuming the microcavity is surrounded by air, the refraction intensity coefficient T can be calculated by $1 - [\sin(\chi - \chi_t)/\sin(\chi + \chi_t)]^2$, where χ_t stands for the angle of refraction given by Snell's law $n\sin\chi = \sin\chi_t$. In the case of the closed cavity, the ray trajectory can visit the entire phase space after an enough time because of the full chaos property of SOS. However, all rays in this dielectric microcavity will refract out in a limited time, arising from a finite refractive index of microcavity. Thus, we can collect the refraction rays and obtain the far-field intensity (namely, emission) distribution as a function of the far-field angle φ.

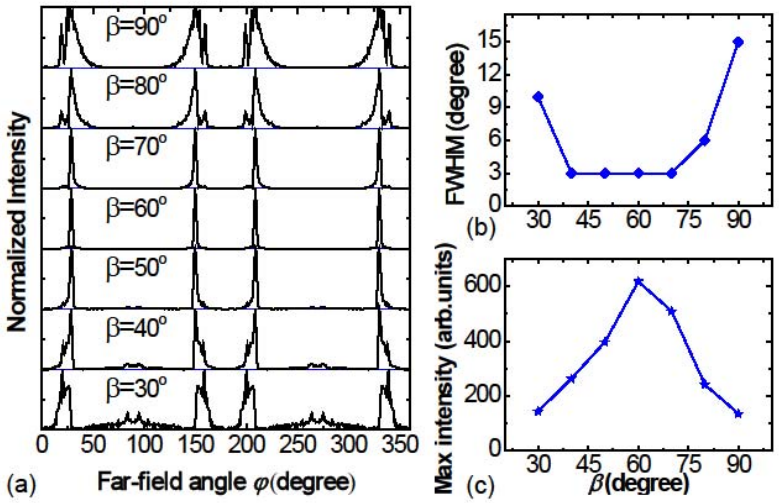

Fig. 2. (Color online) (a) Normalized far-field emission patterns in the cases of different shape setting angle β. (b)-(c) FWHM, i.e., divergence angle, and maximum far-field intensity of one emission peak vs. β.

The initial ensemble of rays is chosen to be uniformly spread in the top area of the phase space ($0.93 < |\sin\chi| < 1$), as we are interested in the relatively high-Q modes of peanut-shaped microcavities. To be consistent with Ref. [19], the refraction index of the present microcavity n is given as 1.52. For different n, it will be discussed in Section V. The similar FFPs with different shape setting angle β are shown in Fig. 2(a). Clearly, in spite of the full chaos in SOS, the peanut-shaped microcavity supports four highly directional emission angles around $\varphi = 29^{o}$, 151^{o}, 209^{o}, and 331^{o}. It is of importance that the divergence angle, defined as the FWHM of the peak in FFP, ranges from 2.5^{o} to 15^{o} (see Fig. 2(b)) approximately. Evidently, Figs. 2(b) and 2(c) indicate that there exist an optimized $\beta \sim 60^{o}$ ($r_1 \sim r_2$) to achieve both the minimized divergence and the maximum far-field intensity. This case is named as the *regular peanut-shaped microcavity*. It should be noted that, for our simplified peanut cavity model, the main features of

FFP obtained from ray dynamics agrees well with the experiment [19].

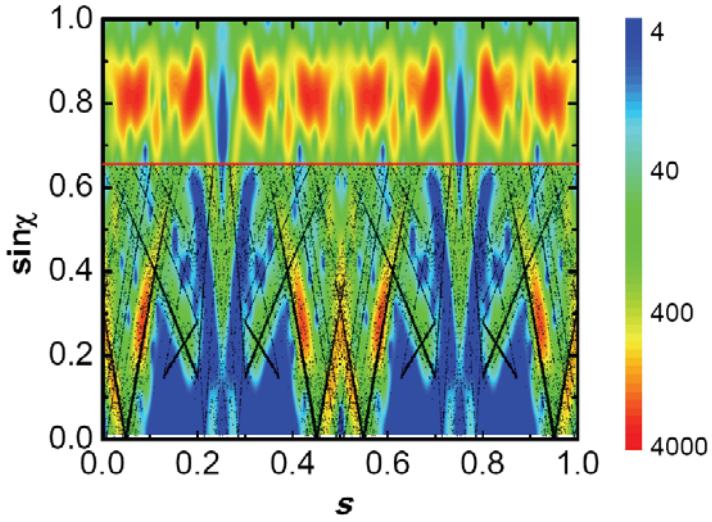

Fig. 3. (Color online) Black dots: Simulations of short-term ray dynamics below the critical refraction line ($\sin\chi_c = 1/n$), for random initial rays with $\sin\chi_c > 0.95$ reflect on the boundary for 60 iterations. Rainbow color: Husimi distribution for a double-pentagons mode (shown in Fig. 4(a)) projected onto the SOS of the deformed microcavity. Here, $\beta = 60^o$.

In the following, we focus on the *regular peanut-shaped microcavity*. Figure 3 plots unstable manifolds (black dots) of the SOS below the critical refraction line ($\chi = \chi_c$), to explain this directional emission that occurs at certain angles. In these manifolds, four noticeable "V"-type lines comprised of dense black dots are present, which indicates rays tend to refract out of the microcavity along them. It is important that the positions of them match well with the four main peaks in the FFP shown in Fig. 2(a).

A lens model [9] is helpful to understand the highly collimated emission of the peanut-shaped microcavity. As shown in the inset of Fig. 4(b), rays tend to emit from an equivalent point light source before they reflect to the fourth quadrant and finally refract out of the microcavity. As the approximate point source is on the focal plane of the spherical lens which

is played by the lower-right boundary, the refracted light behaves collimated. This result is similar to the scatter-induced directional emission [22].

IV. Wave correspondence

Using the boundary element method [23], we obtain all resonances in the range $119 < nkr_1 < 121$, where $k = 2\pi/\lambda$ and λ is the resonance wavelength. Therein, high-Q resonances will be excited as lasing modes with low threshold in practice. The highest Q approaches one thousand, and the corresponding field distribution is shown in Fig. 4 (a). Not like the preliminary interpretation in the experimental literature [19], here we find the resonance is a double-pentagon mode (black line is guided to eyes in Fig. 4(a)). The FFP of this double-pentagon mode is also shown in Fig. 4(b). It agrees well with both the ray trajectory simulation in Fig. 2(a) and the experiment in Ref. [19].

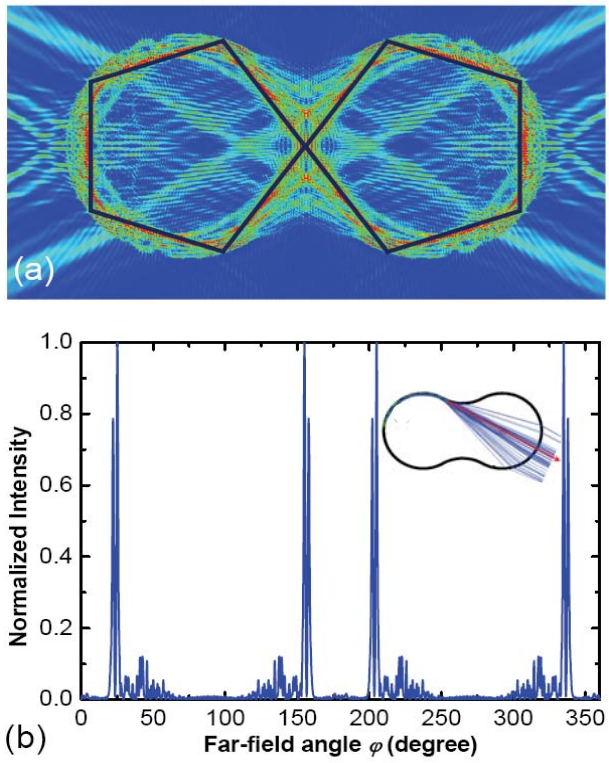

Fig. 4. (Color online) (a) Near-field pattern of double-pentagon mode in real space. The black line marks the eye-guided periodic orbit. (b) The far-field emission pattern for the peanut-shaped cavity with n = 1.52 and β = 60°. Inset: Brief illustration of lens model.

To further study the properties of this double-pentagon mode, we perform the Husimi projection [24], which represents the wave analog of the SOS. The logarithm intensity distribution of the Husimi projection is shown in Fig. 3(a) (rainbow color). In the region above the critical refraction line ($\chi = \chi_c$, red line), eight scars at appropriate positions do exist. It demonstrates the double-pentagon mode even in the fully chaotic peanut-shaped microcavity. In the leaky region, the Husimi projection is also in good agreement with the unstable manifold in detail, and confirms the lens model for high collimated emission.

Evidently, the double-pentagon orbit in our simulation is significantly different from the hybrid WGM-two-bouncing orbit in Ref. [19]. In order to identify the mechanism of the collimated directional emission, we calculate the corresponding free space range $\Delta\lambda$ (FSR), using parameters from the experiment: n = 1.46, λ = 588 nm, r_1 = 64.5 μm. The FSRs are ~ 0.31 nm and ~ 0.32 nm for the double-pentagon orbit and the hybrid WGM-two-bouncing orbit, respectively. Both of them are consist with the experiment $\Delta\lambda$ ~ 0.3 nm.

Though the FSR is similar, the double-pentagon mode can be distinguished from the hybrid WGM-two-bouncing orbit by observing the near-field and far-field intensity patterns simultaneously [25] in future experiments. The secondary peaks in the FFP are emitted from the both ends of the cavity in double-pentagon mode (see Fig. 4(a)), which is very different from the joint emission point of the main and the secondary peaks claimed by the hybrid

WGM-two-bouncing orbit.

V. Discussions

As demonstrated above, the peanut-shaped microcavity owns the merit of high collimation. Here some brief discussions are provided to improve its performances for extensive use. In general, the output performance of deformed microcavity strongly depends on both the cavity geometry and the refraction index of material. In Section II we have defined one morphology parameter β. Actually, if the two circles $C_{1,2}$ are not contacted, the gap between them becomes another morphology parameter. The gap also plays a significant role in the directional emission of the peanut-shaped cavity, determining the directions and divergence, similar to the case that in a stadium-shaped microcavity [9]. In addition, if the two circles are not identical, the radii ratio is another morphology parameter. In this case, the four-fold symmetry of the regular peanut-shaped microcavity is destroyed and the optical vernier effect [26] will appear for the mode which travels both kernels of the peanut.

In the discussion above, the refraction index n of the cavity material is assumed as 1.52. Now we turn to study the emission property with the changing of n. On one hand, Fig. 5(a) depicts the divergence angle with $\beta = 45^o$, 60^o and 75^o. It is found that in the peanut-shaped microcavities, the highly collimated emission appears at the range of low n. The minimized divergence angle is produced at $n \sim 1.5$. When n is larger than 2.2, the divergence angle even exceeds 60^o in the case of $\beta = 45°$, because the two central peaks may overlap each other (see Fig. 5(a) the inset). On the other hand, a bright far-field point is of the essence. To evaluate the

brightness, we obtain the highest intensities in FFPs at the different n, as shown in Fig. 5(b). It can be found that there has an ideal n that lies in low index region for each β. Note that for the regular peanut-shaped microcavity, the ideal refraction index is about 1.52. The peak intensity approaches 633 units with the total initial intensity of 8000 units in ray trajectory. In other words, about 8% energy is concentrated in the angle of one degree. This is 28 times of isotropy emitting energy. If the receptor has ~ 3° flare angle, the received energy exceeds 20%.

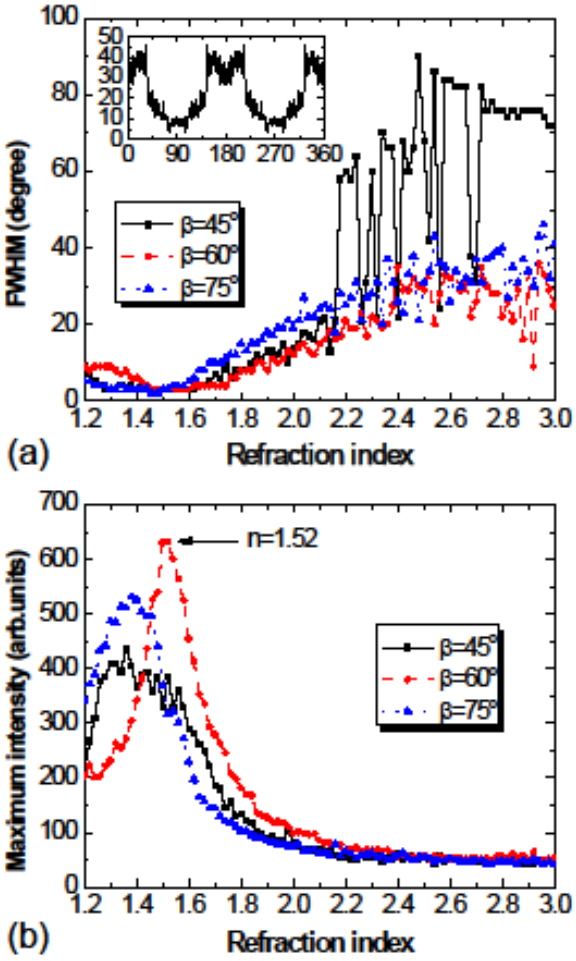

Fig. 5. (Color online) FWHM of main peaks (a) and maximum far-field intensities (b) depending on the

refraction index n with $\beta = 45^o$, 60^o and 75^o. The inset indicates that the two central peaks may overlap when n is higher than 2.2 in the case of $\beta = 45^o$.

VI. Conclusion

In summary, we have theoretically studied the properties of directional emission of a type of peanut-shaped microcavity. The short-term dynamics in ray simulations points out that the deformed microcavity support four evident emission directions. The performed wave simulation also shows the resonance pattern and Husimi projection, and double-pentagon orbit is appeared though the peanut-shaped microcavity is fully chaotic. The FFP obtaining from the wave simulation agrees well with the result given by ray and experiment. Remarkably, this orbit is different from the explanation in Ref. [19], which could be identified by further experiments. The extremely narrow divergence of the emission holds a great potential in highly collimated lasing from on-chip microcavities.

Acknowledgments

This work was supported by the Foundation of He'nan Educational Committee (No. 2011A140021), the Basic and High-tech Project of He'nan Province, and the Youth Foundation of Shangqiu Normal University (No. 2010QN15). YFX acknowledges support from the National Science Foundation of China (No. 10821062 and No. 11004003), the National Basic Research Program of China (No. 2007CB307001), and the Research Fund for the Doctoral Program of Higher Education (No. 20090001120004).

References

[1] K. J. Vahala, nature 424, 839 (2003).

[2] T. Harayama1 and S. Shinohara, Laser & Photonics Reviews 5, 247 (2011); Y.-F. Xiao et al., Front. Optoelectron. China 3, 109 (2010).

[3] A. F. J. Levi et al., Appl. Phys. Lett. 62, 561 (1993).

[4] J. U. Nöckel and A. D. Stone, Nature 385, 45 (1997).

[5] C. Gmachl et al., Science 280, 1556 (1998).

[6] A. Mekis, J. U. Nöckel, G. Chen, A. D. Stone, and R. K. Chang, Phys. Rev. Lett. 75, 2682 (1995); R. Schäfer, U. Kuhl, and H.-J. Stöckmann, New J. Phys. 8, 46 (2006).

[7] H. G. L. Schwefel, N. B. Rex, H. E. Tureci, R. K. Chang, and A. D. Stone, J. Opt. Soc. Am. B 21, 923 (2004).

[8] S.-Y. Lee, M. S. Kurdoglyan, S. Rim, and C.-M. Kim, Phys. Rev. A 70, 023809 (2004); W. Fang, A. Yamilov, and H. Cao, Phys. Rev. A 72, 023815 (2005); S. Shinohara, T. Harayama, H. E. Türeci, and A. D. Stone, Phys. Rev. A 74, 033820 (2006); S. Shinohara and T. Harayama, Phys. Rev. E 75, 036216 (2007).

[9] M. Lebental, J. S. Lauret, J. Zyss, C. Schmit, and E. Bogomolny, Phys. Rev. A 75, 033806 (2007).

[10] M. Lebental, J. S. Lauret, R. Hierle, and J. Zyss, Appl. Phys. Lett. 88, 031108 (2006); S. Shinohara, T. Fukushima, and T. Harayama, Phys. Rev. A 77, 033807 (2008).

[11] G. D. Chern et al., Appl. Phys. Lett. 83, 1710 (2003).

[12] A. Tulek and Z. V. Vardeny, Appl. Phys. Lett. 90, 161106 (2007).

[13] S.-B. Lee et al., Phys. Rev. Lett. 88, 033903 (2002); S.-B. Lee et al., Phys. Rev. A 75, 011802 (2007).

[14] S.-B. Lee, J. Yang, S. Moon, J.-H. Lee, and K. An, Appl. Phys. Lett. 90, 041106 (2007).

[15] J. Wiersig and M. Hentschel, Phys. Rev. Lett. 100, 033901 (2008); Q. H. Song et al.,Phys. Rev. Lett. 105, 103902 (2010).

[16] C.-H. Yi, M.-W. Kim, and C.-M. Kim, Appl. Phys. Lett. 95, 141107 (2009).

[17] S. Chang, R. K. Chang, A. D. Stone, and J. U. Nöckel, J. Opt. Soc. Am. B 17, 1828 (2000).

[18] S. Lacey and H. Wang, Opt. Lett. 26, 1943 (2001); S. Lacey, H. Wang, D. H. Foster, and J. U. Nöckel, Phys. Rev. Lett. 91, 033902 (2003); Y.-F. Xiao et al., Opt. Lett. 32, 644 (2007); Y.-F. Xiao et al., Opt. Lett. 34, 509 (2009).

[19] L. Shang, L.-Y. Liu, and L. Xu, Appl. Phys. Lett. 92, 071111 (2008).

[20] M. Bayer et al., Phys. Rev. Lett. 81, 2582 (1998); S. V. Boriskina, Opt. Lett. 31, 338 (2006); J.-W. Ryu and M. Hentschel, Phys. Rev. A 82, 033824 (2010).

[21] M. Born and E. Wolf, Principles of optics (Cambridge University Press, Cambridge, 1999).

[22] Q. Song and H. Cao, Opt. Lett. 36, 103 (2011); Q. J. Wang et al., Proc. Natl. Acad. Sci. USA 107, 22407 (2010).

[23] J. Wiersig, J. Opt. A: Pure. Appl. Opt. 5, 53 (2003); C.-L. Zou et al., J. Opt. Soc. Am. B 26, 2050 (2009).

[24] M. Hentschel, H. Schomerus, and R. Schubert, Europhys. Lett. 62, 636 (2003).

[25] N. B. Rex, H. E. Tureci, H. G. L. Schwefel, R. K. Chang, and A. D. Stone, Phys. Rev. Lett. 88, 094102 (2002).

[26] X. Wu, H. Li, L.-Y. Liu, and L. Xu, Appl. Phys. Lett. 93, 081105 (2008).